Iterative Joint Channel and Data Estimation for Rank-Deficient MIMO-OFDM

Jos Akhtman, Andreas Wolfgang, Sheng Chen and Lajos Hanzo
School of ECS., Univ. of Southampton, SO17 1BJ, UK.
Tel: +44-23-80-593 125, Fax: +44-23-80-593 045
Email: lh@ecs.soton.ac.uk, http://www-mobile.ecs.soton.ac.uk

***Abstract*— In this paper we propose a turbo-detected multi-antenna-multi-carrier receiver scheme. Following the philosophy of the turbo processing, our turbo MIMO-OFDM receiver comprises a succession of detection modules, namely the channel estimator, the space-time detector and the decoder, which iteratively exchange soft bit-related information and thus facilitate a substantial improvement of the overall system performance. In this paper we analyse the achievable performance of the iterative system proposed with the aim of documenting the various design trade-offs, such as the achievable error-rate performance, the attainable data-rate as well as the associated computational complexity. Specifically, we report a virtually error-free performance for a rate-$\frac{1}{2}$ turbo-coded 8x8-QPSK-OFDM system, exhibiting an effective throughput of $8 \cdot 2 \cdot \frac{1}{2}$=8 bits/sec/Hz and having a pilot overhead of only 10%, at SNR of 7.5dB and normalized Doppler frequency of 0.003, which corresponds to a mobile terminal speed of about 65 km/h.**

I. Introduction

Despite the immense interest of both the academic and the industrial research communities, the conception of a practical multiple-input multiple-output (MIMO) transceiver architecture, which is capable of approaching the MIMO channel's capacity in realistic channel conditions remains largely an open problem.

The class of iterative decision directed channel estimation (DDCE) scemes, where the channel estimation is carried out through a series of iterations utilizing the increasingly-refined soft-decision-based feedback, was explored by Sandell *et. al.* [1], Valenti [2], Yeap *et. al.* [3], Song *et. al.* [4], [5], as well as by Otnes and Tüchler [6], [7]. The closely related class of joint receivers, where the channel parameters and the transmitted information-carrying symbols are estimated jointly was explored for example by Seshadri [8], Baccarelli and Cusani [9], developed further by Knickenberg *et. al.* [10] recently revisited by Cozzo and Hughes [11] as well as Cui and Tellambura [12], [13].

An important overview encompassing most major aspects of broadband MIMO orthogonal frequency division multiplexing (OFDM) wireless communications including both channel estimation and signal detection, as well as time- and frequency-domain synchronization was contributed by Stüber *et al*. [14].

Acknowledgements: The work reported in this paper has formed part of the Wireless Enabling Techniques work area of the Core 4 Research Programme of the Virtual Centre of Excellence in Mobile and Personal Communications, Mobile VCE, www.mobilevce.com, whose funding support, including that of EPSRC, is gratefully acknowledged. Fully detailed technical reports on this research are available to Industrial Members of Mobile VCE.

Other important publications considering MIMO systems operating in realistic channel conditions include those by Münster and Hanzo [15], Li *et. al.* [16], Mai *et. al.* as well as Qiao *et. al.* [17]. Nevertheless, substantial contributions addressing all the major issues pertaining to the design of MIMO transceivers, namely error correction, space-time detection as well as channel estimation in realistic channel conditions remain scarce.

Against this background, in this paper we discuss an iterative, so called *turbo* multi-antenna-multi-carrier (MAMC) receiver architecture. Our turbo receiver is illustrated in Figure 1. Following the philosophy of turbo processing [18], our turbo MIMO-OFDM receiver comprises a succession of detection modules, which iteratively exchange soft bit-related information and thus facilitate a substantial improvement of the overall system performance.

More specifically, our turbo MIMO-OFDM receiver comprises three major components, namely the soft-feedback aided DDCE [7], [19], followed by the soft-input-soft-output (SISO) optimized-hierarchy reduced search algorithm (OHRSA) Log-MAP MIMO detector [20] as well as a classic parallel-concatenated SISO turbo code [21]. Consequently, in this paper we would like to analyze the achievable performance of the entire iterative system. Our aim is to document the various design trade-offs, such as the achievable error-rate performance, the attainable data-rate as well as the associated computational complexity.

The rest of this paper is structured as follows. We commence our discourse with a brief desription of the parallel-concatenated turbo code outlined in Section II-A. Subsequently, in Section II-B we describe the structure of an iterative space-time detector and decoder, where we consider a soft-input-soft-output Log-MAP Optimized Hierarchy Reduced Search Algorithm (OHRSA) space-time decoder in conjunction with the aforementioned parallel-concatenated turbo code. The corresponding BER performance is documented. Finally, in Section II-C we discuss the structure of the entire iterative channel estimation, space-time detection and decoding receiver scheme. In Section III we present an extensive analysis of the achievable BER performance characterizing different aspects of the proposed system's behaviour in realistic channel condition. Specifically, we report a virtually error-free performance for a rate $\frac{1}{2}$ turbo-coded 8x8-QPSK-OFDM system, exhibiting an effective throughput of 8 bits/sec/Hz, while having a pilot overhead of only 10%, at E_b/N_0 of 7.5dB and at a normalized Doppler frequency of 0.003, which corresponds to the mobile

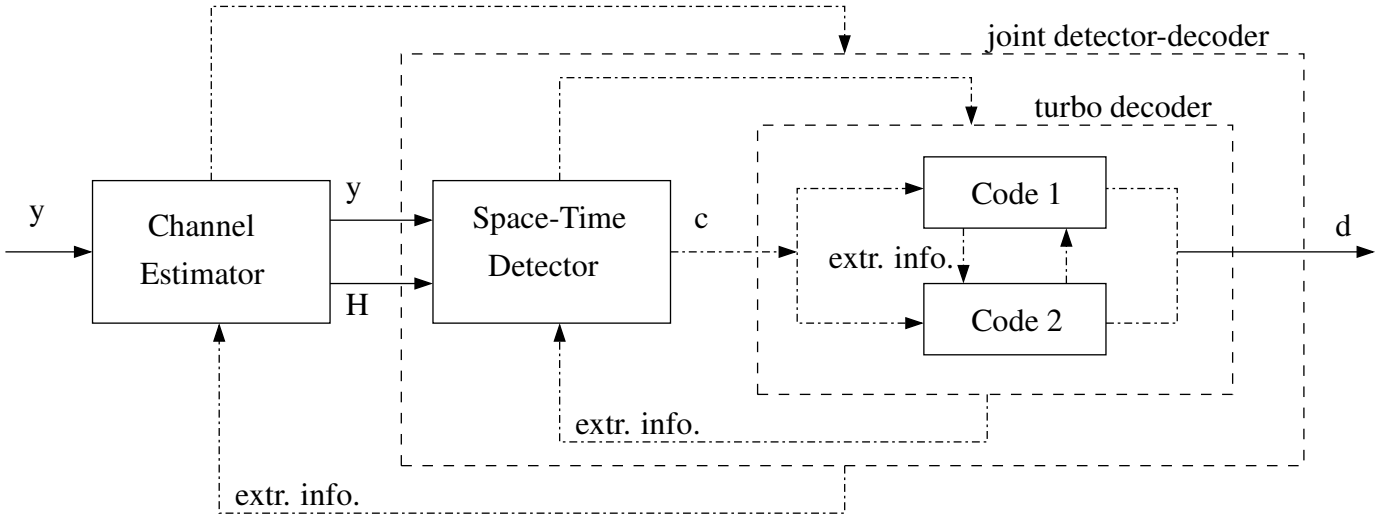

Fig. 1. Schematic of an iterative turbo receiver employing an iterative decision-directed channel estimation, detection and decoding modules.

terminal speed of 65 km/h. Our conclusions are summarised in Section IV.

II. Iterative Receiver Architecture

A. Turbo Forward Error Correction Coding

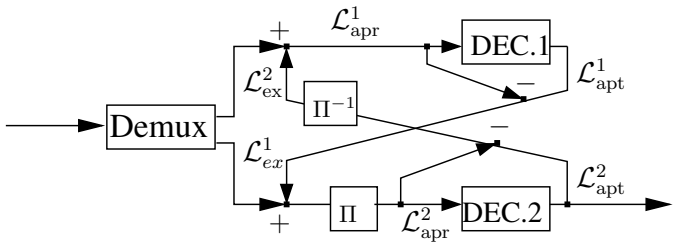

Fig. 2. Scematic of an iterative turbo decoder employing two parallelly-concatenated RSC codes.

The family of the so-called *turbo* codes was first introduced by Berrou *et. al.* [21]–[23]. The properties of turbo codes have been extensively studied in the context of various system architectures by a multiplicity of authors, for instance Benedetto [24], Battail [25], Ömer *et. al.* [26] as well as Hanzo *et. al.* [18]. The plausible conclusion of these studies was that turbo codes are capable of approaching the capacity, while imposing a realistic computational complexity.

Consequently, at the first stage of our iterative turbo receiver architecture illustrated in Figure 1 we employ a turbo decoder. The detailed structure of the turbo decoder considered is depicted in Figure 2. More specifically, our turbo decoder is constituted by a pair of parallel-concatenated soft-input-soft-output (SISO) RSC decoders, which iteratively exchange information-bit-related extrinsic information in the form of LLR values $\mathcal{L}_{\text{ex}}$ for the sake of attaining the highest possible reliability of the decoded information-carrying bits. In this treatise we employed two rate-$\frac{1}{2}$ punctured RSC codes [26]. Observe that the parallel-concatenated codes share the same information bits, while the corresponding parity bits at the output of the encoder are punctured, which results in the overall concatenated code rate of $\frac{1}{2}$. The octally represented RCS generator polynomials of (7,5) having the constraint length of 3 were used for both RCS codes.

The achievable performance of the turbo codes has been thoroughly quantified my multiple authors [18], [23]. Nevertheless, in this section we would like to briefly quantify the achievable BER performance of the specific turbo code considered in the context of increasingly more sophisticated systems communicating under increasingly more realistic channel conditions. Specifically, in Figure 3 we consider the BER performance of the turbo code in the context of a 128-subcarrier OFDM system encountering both uncorrelated Rayleigh fading in the time-domain as well as correlated fading having a time-domain correlation determined by the OFDM-symbol-normalized Doppler frequency spanning the range of $f_D = 0.1$ to 0.003. More specifically, Figure 3 characterizes the achievable BER performance of the turbo decoder considered in the context of a QPSK-modulated OFDM system, while encountering a Rayleigh fading channel exhibiting various correlation properties. For benchmarking purposes, we contrast the performance of a narrow-band system encountering uncorrelated Rayleigh fading as well as that of a $K = 128$-subcarrier OFDM system encountering a dispersive channel having uncorrelated time-domain Rayleigh fading taps specified by the COST-207 Bad Urban (BU) 7-tap CIR [27]. In the frequency-domain this CIR results in a corresponding correlated frequency-selective CTF. Furthermore, we also consider the more realistic scenario of a $K = 128$-subcarrier OFDM system encountering correlated time-domain Rayleigh fading having the Doppler frequencies of $f_D = 0.1, 0.03$ and 0.003 as well as a dispersive CIR characterized by the COST-207 BU model [27].

From Figure 3 we conclude that as expected, while our turbo decoder exhibits a good BER performance [28] in uncorrelated Rayleigh fading, the corresponding BER performance recorded in correlated fading is substantially degraded owing to the relatively low-memory 1000-bit turbo-interleaver, which is unable to break up and randomize the long fading-induced

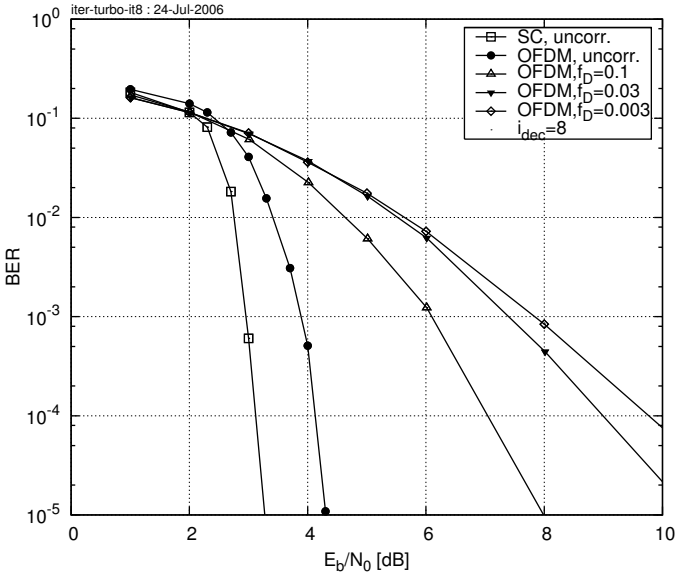

Fig. 3. BER versus E_b/N_0 performance exhibited by the $K = 128$-subcarrier single-antenna QPSK-OFDM system employing a rate $\frac{1}{2}$ parallel-concatenated turbo code in correlated Rayleigh fading having the OFDM-symbol-normalized Doppler frequencies of $f_D = 0.1, 0.03$ and 0.003. The CIR was the 7-path COST-207 BU model [27]. All additional system parameters are summarized in Table I.

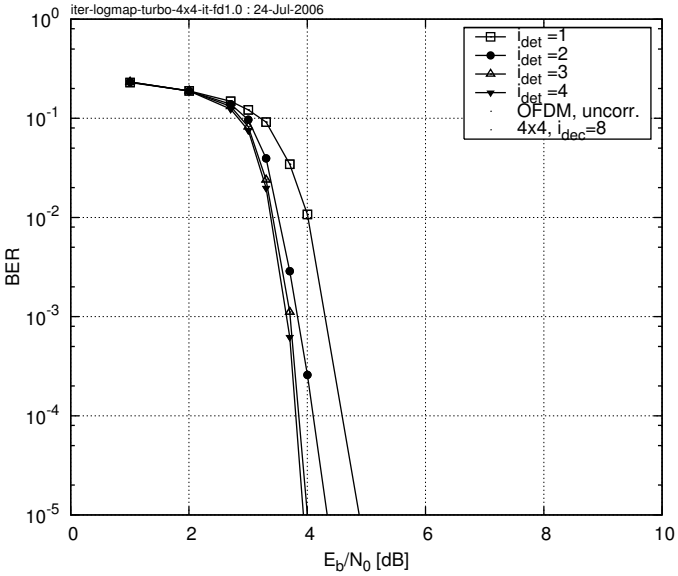

Fig. 5. BER versus E_b/N_0 performance exhibited by the $K = 128$-subcarrier rate $\frac{1}{2}$ turbo-coded 4x4-SDM-QPSK-OFDM system employing the iterative SDM detection and decoding scheme of Figure 4 in uncorrelated time-domain Rayleigh fading channel characterized by the COST-207 BU model [27]. The effective throughput of the system was $4 \cdot 2 \cdot \frac{1}{2} = 4$ bits/sec/Hz. All additional system parameters are summarized in Table I.

error bursts.

B. Iterative Detection – Decoding

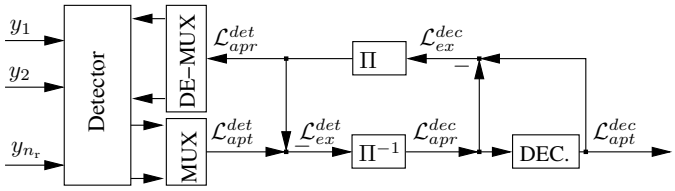

Fig. 4. Schematic of a MIMO receiver employing iterative joint detection and decoding.

Figure 4 portrays the schematic of the iterative space-time detector and decoder considered. Following the philosophy of iterative turbo detection, the incoming subcarrier-related signal vector $\mathbf{y}[n,k]$ is processed by the soft-input-soft-output OHRSA Log-MAP detector described in detail in [20], [29], which delivers the bit-related *a posteriory* LLR values $\mathcal{L}_{\text{apt}}^{\text{det}}$. The resultant LLR values $\mathcal{L}_{\text{apt}}^{\text{det}}$ are then normalized and de-interleaved for the sake of generating the *a priori* bit-related LLR values $\mathcal{L}_{\text{apr}}^{\text{dec}}$, which may be utilized by the turbo decoder of Figure 4. Subsequently, the *a posteriori* LLR values $\mathcal{L}_{\text{apt}}^{\text{dec}}$ generated at the output of the decoder are normalized, interleaved and fed back to the SDM detector in the form of the *a priori* LLR values $\mathcal{L}_{\text{apr}}^{\text{det}}$. This iterative detection process is continued for i_{det} number of detection iterations.

As a next step, we would like to characterize the achievable performance of the iterative SDM detection and decoding scheme illustrated in Figure 4. Throughout this section we stipulate the idealistic assumption of having a perfect knowledge of the OFDM-subcarrier-related CTF.

Firstly, for the sake of benchmarking, in Figure 5 we quantify the BER versus E_b/N_0 performance of the iterative SDM detection and decoding scheme of Figure 4 in the context of a rate-$\frac{1}{2}$ turbo-coded 4x4-SDM-QPSK-OFDM system communicating over the uncorrelated time-domain Rayleigh fading channel characterized by the COST-207 BU model [27]. We consider carrying out $i_{\text{det}} = 1, 2, 3$ and 4 iterations for the SDM detector, while performing $i_{\text{dec}} = 8$ iterations for the inner turbo decoder per each iteration of the SDM detector. From Figure 5 we may observe that an E_b/N_0 gain of about 1 dB is achieved by invoking $i_{\text{det}} = 3$ iterations of the SDM detector and decoder in comparison to invoking a single detection iteration. By contrast, only a minor further E_b/N_0 improvement may be achieved by invoking $i_{\text{det}} > 3$ number of iterations for the SDM detector and decoder complex of Figure 4.

Let us now consider the effects of realistic time-domain correlations encountered by our SDM-OFDM system employing the iterative SDM detection and decoding scheme of Figure 4. Figure 6 characterizes the achievable BER versus E_b/N_0 performance of the iterative SDM detection and decoding scheme, which assumes the iteration pattern of $(i_{\text{det}}, i_{\text{dec}}) = (3, 8)$, in the context of a rate-$\frac{1}{2}$ turbo-coded 4x4-SDM-QPSK-OFDM encountering the OFDM-normalized Doppler frequencies of $f_D = 0.1, 0.03$ and $f_D = 0.003$. The corresponding BER performance recorded in the uncorrelated time-domain Rayleigh fading conditions when using the 7-path COST-207 BU CIR is also shown for the sake of benchmarking. We may observe from Figure 6 that the BER performance exhibited by the system encountering a realistic OFDM-symbol-normalized Doppler frequency of $f_D = 0.003$ lies within an E_b/N_0 range of 0.8 dB from the corresponding BER curve exhibited by

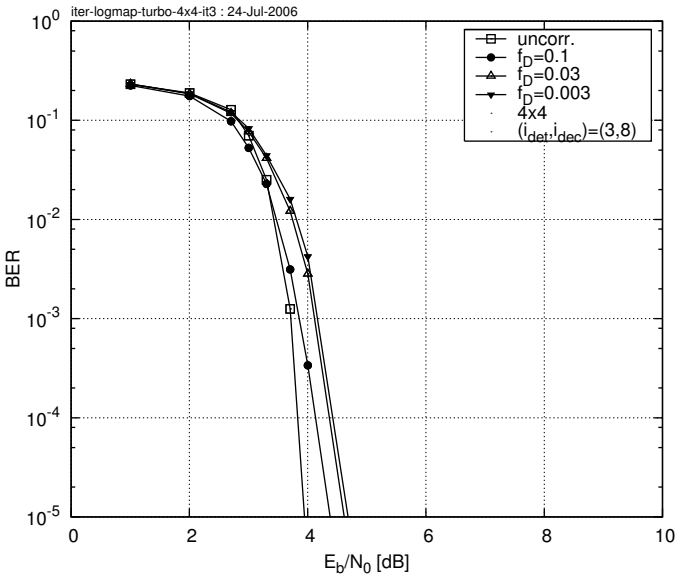

Fig. 6. BER versus E_b/N_0 performance exhibited by the rate-$\frac{1}{2}$ turbo-coded 4x4-SDM-QPSK-OFDM system employing the iterative SDM detection and decoding scheme of Figure 4 in realistic correlated Rayleigh fading conditions when using the 7-path COST-207 BU CIR [27] and encountering the Doppler frequencies of $f_D = 0.1, 0.03$ and 0.003. The BER performance recorded in case of uncorrelated time-domain Rayleigh fading is also shown for the sake of benchmarking. We invoked an iteration pattern of $(i_{\text{det}}, i_{\text{dec}}) = (3, 8)$. The overall throughput was $4 \cdot 2 \cdot \frac{1}{2} = 4$ bits/sec/Hz. Additional system parameters are summarized in Table I.

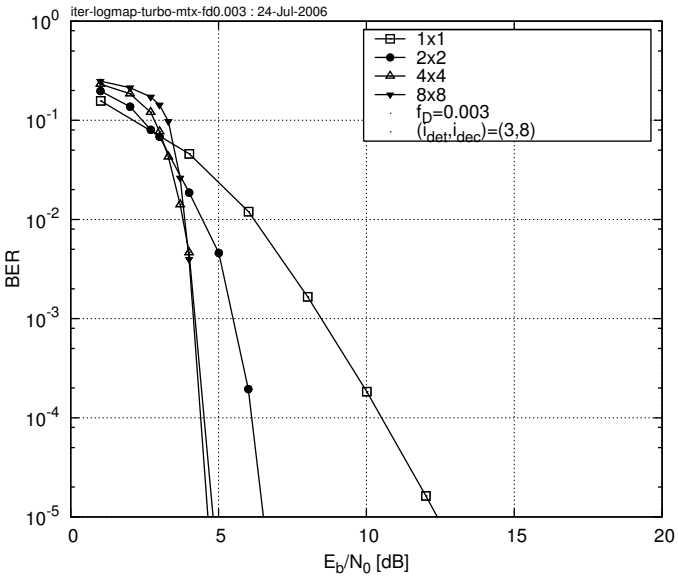

Fig. 7. BER versus E_b/N_0 performance exhibited by the rate-$\frac{1}{2}$ turbo-coded SDM-QPSK-OFDM system employing the iterative SDM detection and decoding scheme of Figure 4 and having $m_{\text{t}} = n_{\text{r}} = 1, 2, 4$ and 8 transmit and receive antennas. We invoked an iteration pattern of $(i_{\text{det}}, i_{\text{dec}}) = (3, 8)$. The 7-path COST-207 BU channel model [27] was used and we assumed encountering the OFDM-symbol-normalized Doppler frequency of $f_D = 0.003$. The overall throughput was 1,2,4 and $8 \cdot 2 \cdot \frac{1}{2} = 8$ bits/sec/Hz, respectively. Additional system parameters are summarized in Table I.

the system encountering idealistic uncorrelated time-domain Rayleigh fading conditions, when using the 7-path COST-207 BU CIR. We may hence conclude that, as expected, our 4x4-SDM-QPSK-OFDM system efficiently exploits the spatial-diversity potential inherent in the MIMO channel.

This conclusion is further supported by the results depicted in Figure 7, where we plot the BER versus E_B/N_0 performance exhibited by the rate-$\frac{1}{2}$ turbo-coded SDM-QPSK-OFDM system employing the iterative SDM detection and decoding scheme of Figure 4 and having $m_{\text{t}} = n_{\text{r}} = 1, 2, 4$ and 8 transmit and receive antennas. We assumed encountering an OFDM-symbol-normalized Doppler frequency of $f_D = 0.003$, while employing bit-interleaving across $N_d = 10$ OFDM symbols. Observe that having an interleaved block of bits spanning the duration of $N_d T_s = 10\ T_s$, which is substantially shorter than channel's coherence time of $1/f_D \approx 300\ T_s$ corresponds to having virtually no time-domain diversity gain. In other words, a relatively short interleaver is unable to break up and randomize the long fading-induced error bursts. Consequently, we may conclude from Figure 7 that the BER performance exhibited by the single-antenna OFDM system is limited by the probability of occurrence of a precipitated burst of errors in some of the OFDM symbols, which we may refer as an *outage* [28] inherent in single-antenna Rayleigh fading channels. On the other hand, SDM-OFDM systems operating in MIMO scenarios exhibit a BER performance, which improves upon increasing the number $m_{\text{t}} = n_{\text{r}}$ of transmit and receive antennas.

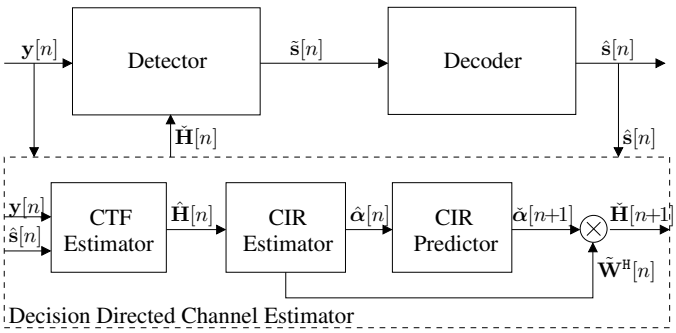

Fig. 8. Schematic of a generic receiver employing DDCE scheme constituted by an *a posteriori* decision-directed CTF Estimator, followed by a CIR Estimator and an *a priori* CIR predictor.

C. Channel Estimation for MIMO-OFDM

The schematic of the channel estimation method considered is depicted in Figure 8. Our channel estimator, which is discussed in detail in [19], is constituted by a soft-input *a posteriori* decision-directed channel transfer function (CTF) estimator [7] followed by a projection approximation subspace tracking (PAST)-aided [30] channel impulse response (CIR) estimator [31] and an *a priori* CIR predictor [31]. As seen in Figure 8, the task of the CTF estimator is to calculate the soft-decision aided temporary estimates $\check{\boldsymbol{H}}[n]$ of the CTF coefficients. Subsequently, the task of the CIR estimator is to track the estimates $\hat{\alpha}_l[n]$ of the CIR taps, which are then fed into the low-rank time-domain CIR tap predictor of Figure 8 for the sake of producing an *a priori* estimate $\check{\alpha}_l[n+1]$, $l = 0, 1, \cdots, L$ of the next CIR on a CIR tap-by-tap basis [31]. Finally, the predicted CIR is converted to the CTF with the aid

of the tranformation matrix $\boldsymbol{W}[n]$ of Figure 8. The resultant CTF is employed by the receiver for the sake of detecting and decoding of the next OFDM symbol.

D. Iterative Channel Estimation – Detection – Decoding

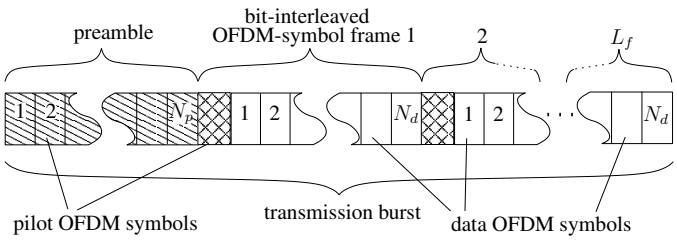

Fig. 9. OFDM transmission burst structure comprising a preamble of N_p full-pilot OFDM symbols followed by a sequence of L_f data OFDM-symbol frames. Each data OFDM-symbol frame is preceded by a single full-pilot OFDM symbol followed by N_d information-carying OFDM symbols. Consequently, our OFDM transmission burst accommodates a total number of $N_p + L_f$ full-pilot OFDM symbols as well as a total number of $L_f N_d$ information-carrying OFDM symbols.

In this paper we consider the transmission of a sequence of consecutive MIMO-OFDM transmission *bursts*, which are processed independently. In other words, each of the self-contained MIMO-OFDM transmission bursts includes all the necessary data, such as for instance pilot signals, required for successful detection and decoding of the information accommodated by the burst. Correspondingly, each MIMO-OFDM transmission burst may be processed independently of the neighbouring bursts. This philosophy is reminiscent of the packet-based transmission scheme adopted, for example, in the IEEE 802.11 a/g WLAN standard [32]. The structure of a single MIMO-OFDM transmission burst considered is depicted in Figure 9. More specifically, our OFDM transmission burst portrayed in Figure 9 commences with a channel-sounding preamble formed by N_p number of pure pilot MIMO-OFDM symbols. Subsequently, our MIMO-OFDM transmission burst accommodates a sequence of $L_f$number of so-called OFDM-symbol-frames. More explicitely, as seen in Figure 9, each OFDM-symbol-frame constitutes a single bit-interleaved turbo-encoded codeword and comprises a single full-pilot MIMO-OFDM symbol followed by N_d number of information-carrying MIMO-OFDM symbols.

For each MIMO-OFDM transmission burst the detection process commences with the initialization of the channel estimator by utilizing the pilot MIMO-OFDM symbols constituting the burst's preamble, as seen in Figure 9. Specifically, both the received signals $\mathbf{y}[n]$ as well as the corresponding transmitted signals $\mathbf{s}[n]$ associated with the N_p pilot MIMO-OFDM symbols constituting the burst preamble of Figure 9 are sequentially fed into the channel estimator of Figure 8 for the sake of attaining an initial convergence for the three adaptive filters constituting the decision-directed channel estimator of Figure 8.

During the first iteration of the detection process, which is carried out for each subsequent N_d-OFDM-symbol data-frame of Figure 9 that commences with a full-pilot MIMO-OFDM symbol associated with the MIMO-OFDM-symbol index n, we perform a long-term prediction of the CIR-related taps using the CIR tap predictor of Figure 8. More specifically, we aim for predicting the CIR associated with the *last* OFDM symbol of the current OFDM-symbol-frame of Figure 9, namely the one associated with the MIMO-OFDM-symbol index of $(n + N_d)$. The CIRs associated with the remaining $(N_d - 1)$ MIMO-OFDM symbols hosted by the current OFDM-symbol-frame are then obtained using linear interpolation between those associated with the nth pilot MIMO-OFDM symbol preceding the current OFDM-symbol-frame and the predicted CIR associated with the last $(n + N_d)$ data OFDM symbol. The predicted and interpolated MIMO-CTF coefficients $\check{\mathbf{H}}[m],\ m = n+1, \ldots, n+N_d$ are utilized for the sake of performing an initial detection of the information-carrying data MIMO-OFDM symbols $\mathbf{s}[n]$.

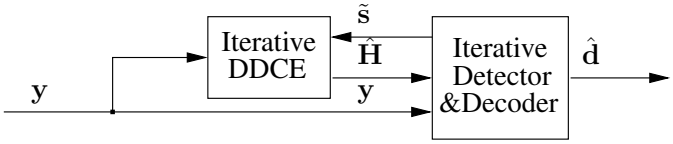

Fig. 10. Schematic of an iterative turbo receiver employing the iterative decision-directed channel estimator of Figure 8 as well as the iterative detection and decoding module.

The resultant tentative estimates of the data-bits $\mathbf{d}$, as well as the associated soft-bit information, corresponding to the entire data MIMO-OFDM-symbol frame of Figure 9 are remodulated in order to generate the soft reference signal $\tilde{\mathbf{s}}[m],\ m = n+1, \ldots, n+N_d$ [7]. The reference signal $\tilde{\mathbf{s}}[m]$ is fed back to the soft-input channel estimator [7] for the sake of refining the estimates of the CTF coefficients $\mathbf{H}[m],\ m = n+1, \ldots, n+N_d$. The interaction between the soft-input channel estimator and the iterative MIMO detection and decoding module is illustrated in Figure 10. The iterative channel estimation–detection–decoding process portrayed in Figure 10 is repeated, until a sufficiently reliable detected MIMO-OFDM symbol $\hat{\mathbf{s}}$ is generated.

E. Mitigation of Error Propagation

The main difficulty associated with the decision-directed approach to channel estimation is constituted by the potential error propagation, where the erroneous data decisions result in erroneous channel estimation, which inflicts further precipitated data decision errors, *etc*. In other words, the reliability of the estimated CTF coefficients degrades rapidly in the presence of decision errors routinely occurring in the low SNR region. The resultant degradation of the channel state information accuracy results in further decision errors and ultimately in divergence of the iterative channel estimation – data detection process and in a subsequent avalanche of decision errors. As was pointed out in [7], the *soft feedback* aided RLS CTF estimator is capable of substantially mitigating the effects of error propagation. Nevertheless, ensuring the stability of an iterative channel estimation – data detection system in the presence of data decision errors remains a challenging issue. Consequently, for the sake of mitigating the system's

vulnerability to error-propagation-related instability effects we propose the following method.

Firstly, after each channel estimation and MIMO detection iteration, which is performed on the N_d-MIMO-OFDM symbol data frame of Figure 9, we record the resultant MSE. The joint channel estimation and MIMO detection MSE may be expressed as follows

$$e^i[n] = \sum_{m=n+1}^{n+N_d} \sum_{k=1}^{K} \|\mathbf{y}[m,k] - \hat{\mathbf{H}}^i[m,k]\hat{\mathbf{s}}^i[m,k]\|^2, \quad (1)$$

where, as before, $\mathbf{y}[m,k]$ denotes the MIMO signal associated with the kth subcarrier of the mth MIMO-OFDM symbol and recorded at the n_r receive antennas, while $\hat{\mathbf{H}}^i[m,k]$ and $\hat{\mathbf{s}}^i[m,k]$ are the corresponding estimates of the CTF coefficient matrix and the transmitted signal vector, which were obtained after the ith iteration of the channel estimation and detection process.

Subsequently, after carrying out i_ce number of channel estimation iterations we select the particular pair of CTF estimates $\hat{\mathbf{H}}^i[m,k]$ and data estimates $\hat{\mathbf{s}}^i[m,k]$, which correspond to the specific iteration resulting in the minimum MSE. More explicitely, the decision rule employed may be expressed as

$$\left\{\hat{\mathbf{H}}[m,k], \hat{\mathbf{s}}[m,k]\right\} = \arg\min_i e^i[n], \quad (2)$$

where we have $m = n+1, \cdots, n+N_d$; $k = 1, \cdots, K$ and $i = 1, \cdots, i_\mathrm{ce}$.

Let us now consider the scenario of encountering a large number of decision errors. Naturally, the decision errors in any of the iterations would result in a degraded channel estimation accuracy in the subsequent iteration and hence even more decision errors as well as an inevitable increase of the corresponding MSE $e^i[n]$. Consequently, invoking the final-decision rule of Equation 2 substantially mitigates the system's *avalanche*-like error propagation and hence improves the system's stability and robustness.

III. Performance Analysis

TABLE I
System parameters.

Parameter	Value
Carrier frequency f_c	2.5 GHz
Channel bandwidth B	8 MHz
Number of carriers K	128
FFT frame duration T_s	16 μs
OFDM symbol duration T	20 μs (4 μs of cyclic prefix)
Max. delay spread τ_{max}	4 μs
Max. terminal speed v	130 km/h
Norm. Max. Doppler spread f_D	0.006 = $T \cdot 300$ Hz

A. Number of Channel Estimation – Detection Iterations

Firstly, we would like to characterize the BER performance gain attained by the iterative MIMO-PAST-DDCE in comparison to single-iteration channel estimation. More specifically, Figure 11 portrayes the BER versus E_b/N_0 performance of the rate 1/2 turbo-coded 4x4-MIMO-QPSK-OFDM system invoking $i_\mathrm{ce} = 1, 2, 3$ and 4 channel estimation iterations as well as $i_\mathrm{det} = 2$ MIMO detector iterations and $i_\mathrm{dec} = 4$ iterations of the parallelly-concatenated turbo decoder per each iteration of the channel estimator. We assumed employing the transmission burst structure depicted in Figure 9, where the corresponding parameters were given by $(L_f, N_p, N_d) = (8, 8, 10)$, which yields an overall pilot overhead of $\varepsilon = (N_p + L_f)/(L_f N_d) = 0.1$, or in other words 10%. The 7-path COST-207 BU channel model was used and we assumed encountering the Doppler frequency of $f_D = 0.003$. As may be concluded from Figure 11, the MIMO-OFDM system proposed exhibits an E_b/N_0 gain of about 2 dB, when comparing three iterations and a single iteration of the channel estimator. Moreover, only a modest further E_b/N_0 gain may be achieved upon invoking a higher number of channel estimation iterations.

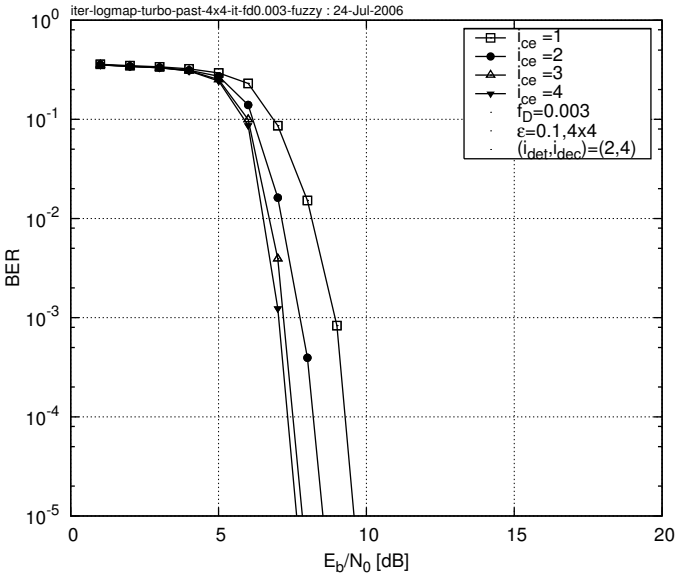

Fig. 11. BER versus E_b/N_0 performance exhibited by the rate-$\frac{1}{2}$ turbo-coded 4x4-MIMO-4QAM-OFDM iterative turbo receiver of Figure 10 invoking $i_\mathrm{ce} = 1, 2, 3$ and 4 channel estimation iterations as well as $(i_\mathrm{det}, i_\mathrm{dec}) = (2, 4)$ MIMO detection and turbo decoding iterations, respectively. The 7-path COST-207 BU channel model [27] was used and we assumed encountering the OFDM-symbol-normalized Doppler frequency of $f_D = 0.003$. The effective throughput was $4 \cdot 2 \cdot \frac{1}{2} = 4$ bits/sec/Hz. All additional system parameters are summarized in Table I.

B. Pilot Overhead

In order to provide further insights, Figure 12 characterizes the achievable BER versus E_b/N_0 performance exhibited by the 4x4-MIMO-QPSK-OFDM turbo receiver of Figure 10 employing different m_t and n_r numbers of transmit and receive antennas. Specifically, we consider invoking $(i_\mathrm{ce}, i_\mathrm{det}, i_\mathrm{dec}) = (3, 2, 4)$ channel estimation, detection and decoding iterations, respectively, while employing $m_\mathrm{t} = n_\mathrm{r} = 1, 2, 4, 6$ and 8 transmit and receive antennas. Observe, that the BER performance improves rapidly upon increasing the $m_\mathrm{t} = n_\mathrm{r}$ number of transmit and receive antennas, as long as it does not exceed $m_\mathrm{t} = n_\mathrm{r} = 4$. Furthermore, the BER performance degrades slowly upon further increasing the number of antennas according to $m_\mathrm{t} = n_\mathrm{r} > 4$. The simple explanation of this

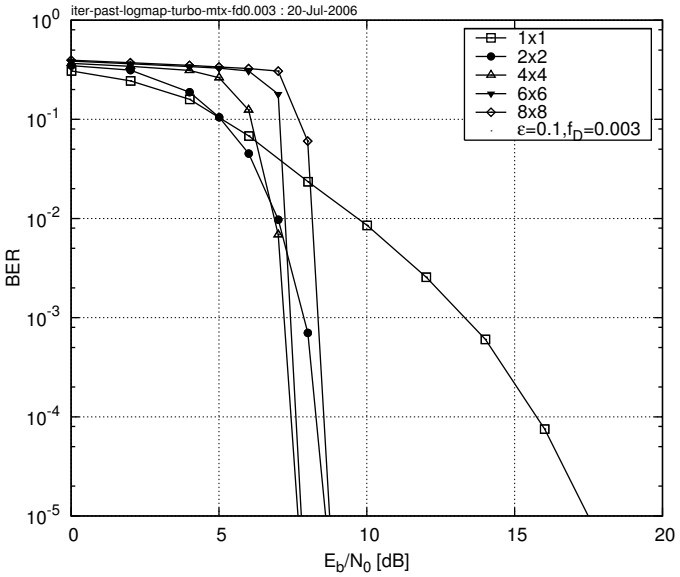

Fig. 12. The BER versus E_b/N_0 performance exhibited by the rate-$\frac{1}{2}$ turbo-coded MIMO-QPSK-OFDM turbo receiver of Figure 10 using $m_{\rm t} = n_{\rm r} = 1, 2, 4, 6$ and 8 transmit and receive antennas. The corresponding effective throughputs were $1, 2, 4, 6$ and $8 \cdot 2 \cdot \frac{1}{2} = 8$ bits/sec/Hz, respectively. The 7-path COST-207 BU channel model was used [27] and we assumed encountering the Doppler frequency of $f_D = 0.003$. The pilot overhead of 10% and the iteration pattern of $(i_{\rm ce}, i_{\rm det}, i_{\rm dec}) = (3, 2, 4)$ were used. Additional system parameters are summarized in Table I.

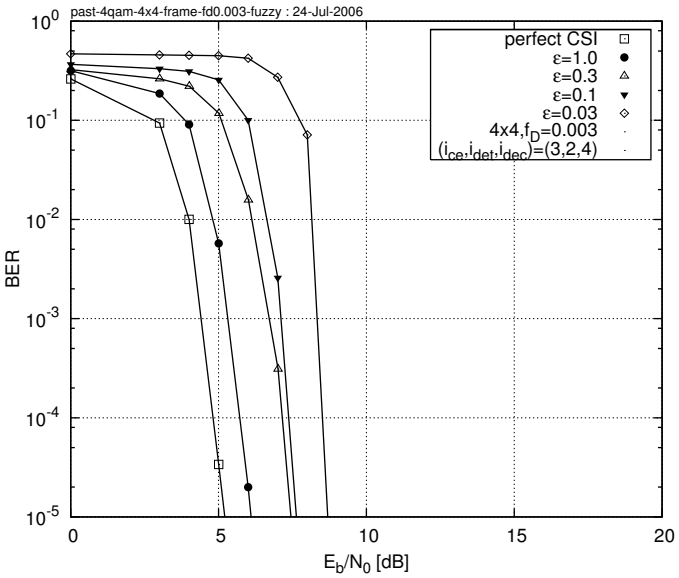

Fig. 13. BER versus E_b/N_0 performance exhibited by the rate-$\frac{1}{2}$ turbo-coded 4x4-MIMO-QPSK-OFDM turbo receiver of Figure 10. The pilot overhead was either 3, 10, 30, or 100%, which corresponds to $\varepsilon = 0.03, 0.1, 0.3$ and 1.0, respectively, where we consider the idealistic scenario of having 100% pilots as well as the scenario of perfect channel state information for benchmarking purposes. The 7-path COST-207 BU channel model [27] was used and the Doppler frequency was $f_D = 0.003$. The iteration pattern of $(i_{\rm ce}, i_{\rm det}, i_{\rm dec}) = (3, 2, 4)$ was used and the effective throughput was $4 \cdot 2 \cdot \frac{1}{2} = 4$ bits/sec/Hz. All additional system parameters are summarized in Table I.

phenomenon is that as expected, the MIMO-OFDM system benefits from the increased spatial diversity associated with a higher number of antennas. On the other hand, as noted in Section II-C, the channel estimation problem becomes increasingly more rank-deficient and hence the estimation accuracy of the CIR taps as well as the corresponding subcarrier-related CTF coefficients degrades upon increasing the number of independent spatial links constituting the MIMO channel. The overall system performance is determined by the associated trade-off between the beneficial diversity gain increase and the inevitable degradation of the estimated CTF accuracy. Ultimately, however, the deterioration of the estimated CTF accuracy does not appear to constitute a major impediment. Quantitatively, as evidenced by the results of Figure 12, the BER performance exhibited by the high-complexity system having $m_{\rm t} = n_{\rm r} = 8$ antennas lies within a 1 dB margin in comparison to the corresponding BER performance curve associated with the system having $m_{\rm t} = n_{\rm r} = 4$ transmit and receive antennas. Observe that the 4x4 system exhibits the best recorded performance and hence appears to represent an optimum tradeoff between the beneficial special diversity gain and the system-size-related channel estimation accuracy degradation.

C. Performance of a Symmetric MIMO System

Subsequently, we would like to characterize the achievable BER performance exhibited by the MIMO-QPSK-OFDM turbo receiver of Figure 10 using various densities of the dedicated pilot MIMO-OFDM symbols. More specifically, in Figure 13 we have plotted the rate $1/2$ turbo-coded QPSK-related BER exhibited by our MIMO-OFDM system employing $m_{\rm t} = n_{\rm r}$ transmit and receive antennas. For benchmarking purposes we have included the BER versus E_b/N_0 performance of the MIMO-OFDM system assuming perfect CIR knowledge, as well as assuming channel estimation based on the idealistic scenario of having 100% pilots. Furthermore, we present our results for the MIMO-OFDM system using pilot overheads of 30, 10 and 3%, which corresponds to the pilot overhead ratio of $\varepsilon = 0.3, 0.1$ and 0.003, respectively. We observe from Figure 13 that the 100% pilot-based channel estimation results in an approximately 1 dB E_b/N_0 degradation in comparison to the perfect CIR estimation scenario. Furthermore, the more realistic assumption of employing up to 10% dedicated MIMO-OFDM pilot symbols results in a further E_b/N_0 degradation of about 1.5 dB in comparison to the 100% pilot-based scenario. Additionally, a further reduction of the pilot overhead to as low as 3% of pilots results in an E_b/N_0 degradation of 2.5 dB in comparison to the 100% pilot-based scenario.

1) Performance of a Rank-Deficient MIMO System: Similar phenomena may be observed in Figure 14, which characterizes the achievable BER performance exhibited by a rank-deficient 4x2-MIMO-QPSK-OFDM system. The 4x2 MIMO scenario constitutes a particularly interesting detection problem. More specifically, let us consider the kth subcarrier of the nth MIMO-OFDM symbol. The computational challenge lies in the fact that we have to estimate as many as *four* transmitted M-QAM symbols $s_j[n,k],\ j = 1, \ldots, 4$ as well as the corresponding *eight* CTF coefficients $H_{ij}[n,k], i = 1, 2,\ j = 1, \ldots, 4$, while utilising merely the *two* recorded signal samples of $y_i[n,k],\ i = 1, 2$. Consequently, similarly to

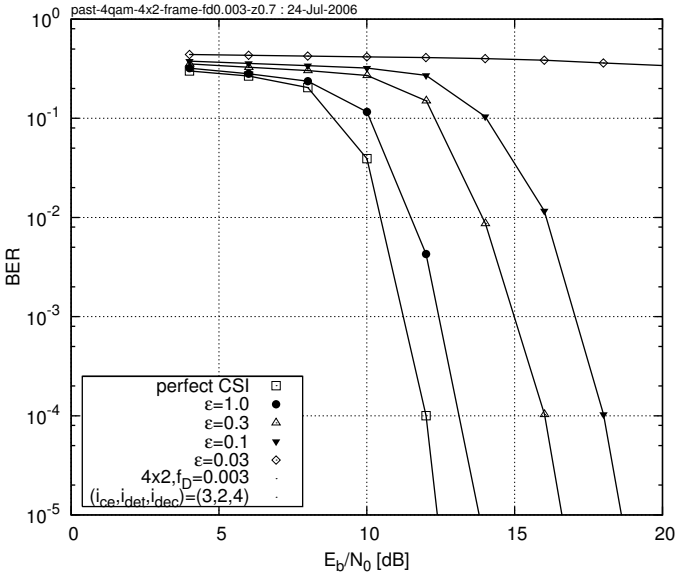

Fig. 14. BER versus E_b/N_0 performance exhibited by the rank-deficient rate-$\frac{1}{2}$ turbo-coded 4x2-MIMO-QPSK-OFDM turbo receiver of Figure 10. The pilot overhead was either 3, 10, 30, or 100%, which corresponds to $\varepsilon = 0.03, 0.1, 0.3$ and 1.0, respectively, where we consider the idealistic scenario of having 100% pilots as well as the scenario of perfect channel state information for benchmarking purposes. The 7-path COST-207 BU channel model was used [27] and the Doppler frequency was $f_D = 0.003$. The iteration pattern of $(i_{\text{ce}}, i_{\text{det}}, i_{\text{dec}}) = (3, 2, 4)$ was used and the effective throughput was $4 \cdot 2 \cdot \frac{1}{2} = 4$ bits/sec/Hz. All additional system parameters are summarized in Table I.

Figure 13 we have plotted the BER versus E_b/N_0 performance of the 4x2-MIMO-QPSK-OFDM system assuming perfect CSI as well as assuming channel estimation based on the idealistic scenario of having 100% pilots. Furthermore, we have plotted the BER corresponding to the scenarios of using pilot overheads of 30, 10 and 3%. Similarly to the 4x4 scenario, assuming 100% pilot-based channel estimation results in an approximately 1 dB E_b/N_0 degradation in comparison to the perfect CIR knowledge scenario. On the other hand, in contrast to the 4x4 scenario characterized in Figure 13, in Figure 14 we may observe that the system employing 10% of dedicated MIMO-OFDM pilot symbols results in nearly 6 dB E_b/N_0 degradation in comparison to the 100% pilot-based scenario. Furthermore, an additional reduction of the pilot overhead to 3% of pilots results in a system instability and hence no satisfactory BER performance may be achieved, regardless of the SNR encountered.

IV. Conclusions

In this paper we have documented the performance trends exhibited by the proposed turbo MIMO-OFDM receiver of Figure 1, which comprises three major components, namely, the soft-feedback decision-directed MIMO channel estimator outlined in Section II-C, followed by the soft-input-soft-output OHRSA Log-MAP MIMO detector [20] as well as a soft-input-soft-output parallel-concatenated turbo code [21]. As seen in Figure 12, we have found that our turbo SDM-OFDM system employing the MIMO-DDCE scheme of Section II-C as well as the OHRSA Log-MAP SDM detector [20] exhibits a virtually error-free performance for a rate-$\frac{1}{2}$ turbo-coded 8x8-QPSK-OFDM system, having an effective throughput of 8 MHz $\cdot$ 8 bits/s/Hz=64 Mbps and invoking a pilot overhead of only 10% at SNR of 7.5dB and a normalized Doppler frequency of 0.003, which corresponds to a mobile terminal speed of about 65 km/h[1].

References

[1] M. Sandell, C. Luschi, P. Strauch, and R. Yan, "Iterative channel estimation using soft decision feedback," in *IEEE Global Telecommunications Conference*, vol. 6, Sydney, NSW, 1998, pp. 3728–3733.

[2] M. Valenti, "Iterative channel estimation for turbo codes over fading channels," in *IEEE Wireless Communications and Networking Conference*, vol. 3, 23-28 September 2000, pp. 1019–1024.

[3] B.-L. Yeap, C. Wong, and L. Hanzo, "Reduced complexity in-phase/quadrature-phase M-QAM turbo equalization using iterative channel estimation," *IEEE Transactions on Wireless Communications*, vol. 2, no. 1, pp. 2–10, 2003.

[4] S. Song, A. Singer, and K.-M. Sung, "Turbo equalization with an unknown channel," in *Proceedings of IEEE International Conference on Ascoustics, Speech and Signal Processing*, vol. 3, 2002.

[5] ——, "Soft input channel estimation for turbo equalization," *IEEE Transactions on Signal Processing, [see also IEEE Transactions on Acoustics, Speech and Signal Processing]*, vol. 52, pp. 2885–2894, 2004.

[6] R. Otnes and M. Tüchler, "Soft iterative channel estimation for turbo equalization: comparison of channel estimation algorithms," in *The 8th International Conference on Communication Systems*, vol. 1, 2002, pp. 72–76.

[7] ——, "Iterative channel estimation for turbo equalization of time-varying frequency-selective channels," *IEEE Transactions on Wireless Communications*, vol. 3, no. 6, pp. 1918–1923, 2004.

[8] N. Seshadri, "Joint data and channel estimation using blind trellis search techniques," *IEEE Transactions on Communications*, vol. 42, no. 2/3/4, pp. 1000–1011, February/March/April 1994.

[9] E. Baccarelli and R. Cusani, "Combined channel estimation and data detection using soft statistics for frequency-selective fast-fading digital links," *IEEE Transactions on Communications*, vol. 46, no. 4, pp. 424–427, Apr. 1998.

[10] A. Knickenberg, B.-L. Yeap, J. Hàmorskỳ, M. Breiling, and L. Hanzo, "Non-iterative Joint Channel Equalisation and Channel Decoding," *IEE Electronics Letters*, vol. 35, no. 19, pp. 1628–1630, 16 September 1999.

[11] C. Cozzo and B. Hughes, "Joint channel estimation and data detection in space-time communications," *IEEE Transactions on Communications*, vol. 51, no. 8, pp. 1266–1270, Aug. 2003.

[12] T. Cui and C. Tellambura, "Joint channel estimation and data detection for OFDM systems via sphere decoding," in *Proceedings of IEEE Global Telecommunications Conference*, vol. 6, 29 Nov.-3 Dec. 2004, pp. 3656–3660.

[13] ——, "Joint data detection and channel estimation for OFDM systems," *IEEE Transactions on Communications*, vol. 54, no. 4, pp. 670–679, 2006.

[14] G. Stüber, J. Barry, S. McLaughlin, Y. Li, M. Ingram, and T. Pratt, "Broadband MIMO-OFDM wireless communications," *Proceedings of the IEEE*, vol. 92, no. 2, pp. 271–294, Feb 2004.

[15] M. Münster and L. Hanzo, "Parallel-interference-cancellation-assisted decision-directed channel estimation for OFDM systems using multiple transmit antennas," *IEEE Transactions on Wireless Communications*, vol. 4, no. 5, pp. 2148–2162, Sept. 2005.

[16] Y. Li, J. Winters, and N. Sollenberger, "MIMO-OFDM for wireless communications: signal detection with enhanced channel estimation," *IEEE Transactions on Communications*, vol. 50, no. 9, pp. 1471–1477, 2002.

[17] X. Qiao, Y. Cai, and Y. Xu, "Joint iterative decision feedback channel estimation for turbo coded v-BLAST MIMO-OFDM systems," in *IEEE International Symposium on Communications and Information Technology*, vol. 2, 2005, pp. 1384–1388.

[18] L. Hanzo, T. H. Liew, and B. L. Yeap, *Turbo Coding, Turbo Equalisation and Space-Time Coding*. Chichester, UK; Piscataway, NJ, USA: John Wiley and IEEE Press, 2002, 766 pages. (For detailed contents, please refer to http://www-mobile.ecs.soton.ac.uk.).

[19] J. Akhtman and L. Hanzo, "Advanced channel estimation for MIMO-OFDM in realistic channel conditions," in *Proceedings of IEEE International Conference on Communications*, 24-28 June 2007, to appear.

[1] Additional system parameters are characterized in Table I.

[20] ——, "Maximum-Likelihood Advanced Sphere Decoding for MIMO-OFDM," in *OFDM and MC-CDMA: A Primer by L. Hanzo and T. Keller*. New York, USA: John Wiley, 2006, pp. 253–302.

[21] C. Berrou, A. Glavieux, and P. Thitimajshima, "Near shannon limit error-correcting coding and decoding: Turbo codes," in *Proceedings of IEEE International Conference on Communications*. Geneva, Switzerland: IEEE, May 1993, pp. 1064–1070.

[22] C. Berrou and A. Glavieux, "Near optimum error-correcting coding and decoding: Turbo codes," *IEEE Transactions on Communications*, vol. 44, no. 10, pp. 1261–1271, October 1996.

[23] C. Berrou, "Some Clinical Aspects of Turbo Codes," in *Proceedings of the International Symposium on Turbo Codes & Related Topics*, Brest, France, 3-5 September 1997, pp. 26–31.

[24] S. Benedetto, R. Garello, and G. Montorsi, "A search for good convolutional codes to be used in the construction of turbo codes," *IEEE Transactions on Communications*, vol. 46, no. 9, pp. 1101–1105, September 1998.

[25] G. Battail, "A conceptual framework for understanding turbo codes," *IEEE Journal on Selected Areas in Communications*, vol. 16, no. 2, pp. 245–254, 1998.

[26] O. Açikel and W. Ryan, "Punctured turbo-codes for BPSK/QPSK channels," *IEEE Transactions on Communications*, vol. 47, no. 9, pp. 1315–1323, September 1999.

[27] M. Failli, "Digital land mobile radio communications COST 207," European Commission, Tech. Rep., 1989.

[28] A. Goldsmith, S. A. Jafar, N. Jindal, and S. Vishwanath, "Capacity limits of MIMO channels," *IEEE Journal on Selected Areas in Communications*, vol. 21, no. 5, pp. 684–702, June 2003.

[29] J. Akhtman, A. Wolfgang, S. Chen, and L. Hanzo, "An optimized-hierarchy-aided near-LogMAP detector for MIMO systems," *IEEE Trans. on Wireless Communications*, 2007, to appear.

[30] B. Yang, "Projection approximation subspace tracking," *IEEE Transactions on Signal Processing*, vol. 43, no. 1, pp. 95–107, January 1995.

[31] L. Hanzo, M. Münster, B. J. Choi, and T. Keller, *OFDM and MC-CDMA for Broadband Multi-User Communications, WLANs and Broadcasting*. John Wiley and IEEE Press, 2003, 992 pages.

[32] *Wireless LAN Medium Access Control (MAC) and Physical Layer (PHY) specifications*, IEEE 802.11g ed., IEEE LAN/MAN Standards Committee, 2003. [Online]. Available: http://standards.ieee.org/getieee802/802.11.html